Possible topological contribution to the anomalous Hall effect of non-collinear ferromagnet Fe3Sn2

Possible topological contribution to the anomalous Hall effect of non-collinear ferromagnet Fe_3Sn_2

Christopher D. O'Neill,[1] Andrew S. Wills,[2,3] and Andrew D. Huxley[1]

[1]*School of Physics and Astronomy and CSEC, University of Edinburgh, Edinburgh, EH9 3JZ, UK*
[2]*Chemistry Department, UCL, 20 Gordon Street, London WC1H 0AJ, UK*
[3]*London Centre for Nanotechnology, 17-19 Gordon Street, London WC1H 0AH, UK*

(Dated: November 6, 2019)

The magnetisation, magnetoresistance and Hall effect of the kagome structured material Fe_3Sn_2 is reported for high quality single crystals. Previous investigations of Fe_3Sn_2 polycrystals detected ferromagnetism at $T_c \approx 657$ K with moments along the easy c-axis and a moment rotation towards the a-b plane on cooling that culminates in moments freezing to form a spin glass at $T_F \approx 80$ K. The results presented here for single crystals show a lower value of $T_F = 70 \pm 2.5$ K most likely due to the increased sample quality. Above T_F we identify a topological contribution to the Hall resistivity coinciding with an anomalous magnetoresistance. This supports recent proposals that the magnetic structure contains magnetic Skyrmions in this temperature range.

I. INTRODUCTION

Topologically protected quantum phenomena are known to exist in a wide range of condensed matter systems. One such state with promising use in technological applications is the topological Hall effect (THE) in materials with magnetic spin structures that exhibit chirality [1]. It is realisable for materials containing whirls of magnetic spins known as Skyrmions such as MnSi [2] or other complex non-trivial spin structures like those of geometrically frustrated pyrochlores [3]. Electrons passing through the chiral structure acquire a Berry phase contribution that leads to a topological Hall effect in addition to a background from the ordinary Lorentz force Hall effect and anomalous Hall effect (AHE) present in magnetic materials. For large enough effects the THE contribution may be separated from the background effects in transport experiments, for example in MnSi [4, 5].

Here we discuss the Hall effect in metallic Fe_3Sn_2, which has a kagome crystal structure well known in the context of geometrically frustrated magnetic spins. In Fe_3Sn_2 ferromagnetism with non-collinear spins indicative of frustration has been reported [6], while in applied field the presence of Skyrmion like spin textured bubbles has been detected [7, 8]. This makes Fe_3Sn_2 an interesting candidate to look for a THE. We report Hall effect, magnetisation and magnetoresistance measurements on high quality single crystals of Fe_3Sn_2. An extra component of Hall resistivity, $\Delta\rho_{xy}$, can be isolated after subtraction of the ordinary and anomalous Hall effect contributions that bears a striking resemblance to a THE. The existence of $\Delta\rho_{xy}$ is complimented by an anomaly in magnetoresistance over the same temperature and field range.

Fe_3Sn_2 has the space group $R\bar{3}m$ and Fe atoms form kagome planes made up of two sizes of equilateral triangles of side length 2.732 and 2.582 Å, shown as red and blue respectively in Figure 1 (a). The kagome planes form offset bilayers where the smaller Fe-Fe distances make up octahedra, shown in Figure 1 (b). The Sn atoms sit within the kagome layers and between the bilayers [6, 9, 10]. Previous reports using Mössbauer spectroscopy [11–13] and magnetometry [6, 14], detected ferromagnetism with moments along the c-axis below the Curie temperature, T_C ($T_C = 657$ K - 612 K, depending on sample). Upon cooling below 250 K, a continuous rotation of the moments from the c-axis into the a-b plane was detected with Mössbauer spectroscopy [12, 13]. However magnetic susceptibility, (M/H), indicates the rotation begins at a much higher temperature [6]. A change in slope of M/H below ≈ 520 K resembles the onset of a small angle moment rotation and on further cooling a sharper change of slope at ≈ 300 K suggests an abrupt increase in rotation angle for temperatures below. Powder neutron diffraction patterns reveal the moment rotation in Fe_3Sn_2 is non-collinear, consistent with magnetic frustration due to a strong competition between the magnetic interactions present [6]. The competition between magnetic interactions is evidenced further by a a second transition, reminiscent of moments freezing to a spin glass state, at $T_F \approx 80$ K [6]. The exact details of the spin glass state are unknown.

Pereiro *et al.* [15] showed that competing magnetic interactions in a kagome lattice can result in Skyrmion spin structured excitations. Experimentally, it appears that in Fe_3Sn_2 such Skyrmions may be static. The evidence comes from Lorentz transmission electron microscopy in an applied magnetic field, $\mu_0 H$, parallel ($||$) to the c-axis. This revealed striped domains that transformed to magnetic bubbles on increasing field [7]. The bubbles appeared to be made up of concentric rings of varying winding directions, making them topologically equivalent to magnetic Skyrmions [7, 8]. The authors note the bubbles may originate from the uniaxial magnetic anisotropy present in the material rather than the anti-symmetric Dzyaloshinskii-Moriya

interaction responsible for the Skyrmions in MnSi [7, 8]. The presence of Skyrmionic bubbles is seen for fields up to ≈ 1.1 T and a temperature range of 380 K - 130 K [7]. For $\mu_0 H > 1.1$ T all moments were seen to align with the c-axis. We now discuss our results that confirm that there is a topological magnetic Hall signal consistent with the presence of Skyrmions.

II. EXPERIMENT AND RESULTS

Single crystals of Fe_3Sn_2 were grown by chemical vapour deposition from powdered material that had in turn been prepared from the elements. The powder of Fe_3Sn_2 was prepared from stoichiometric quantities of Fe and Sn that were ground together and pressed into a pellet that was placed into a silica ampoule and evacuated to 10^{-5} mbar. Back-filling with argon was carried out to a pressure of 3.5 mbar to reduce Sn evaporation. The ampoule was then heated to 80 °C with a ramp rate of 1 °C min^{-1} and left for 7 days. The reaction was then quenched by submersion in cold water. Single crystals were prepared by chemical vapour transport with 40 mg of iodine as a carrier and 500 mg of the prepared Fe_3Sn_2 powder loaded into a 16 cm long

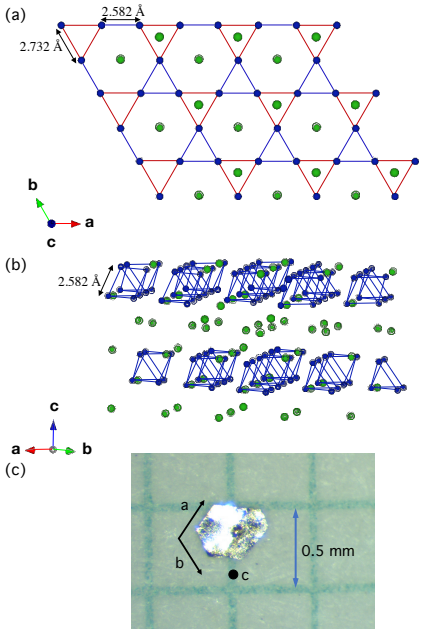

FIG. 1: **(a)** The crystal structure of Fe_3Sn_2 with the crystallographic axes shown as coloured arrows. The blue Fe atoms form kagome planes made up of two sizes of equilateral triangles of 2.732 and 2.582 Å shown as blue and red respectively. **(b)** The kagome planes are bilayered where the 2.582 Å Fe-Fe triangles form octahedra and the green Sn atoms sit within the kagome planes and between bilayers. **(c)** A typical hexagonal crystal of Fe_3Sn_2 showing the directions of the crystallographic axes along with a scale for comparison.

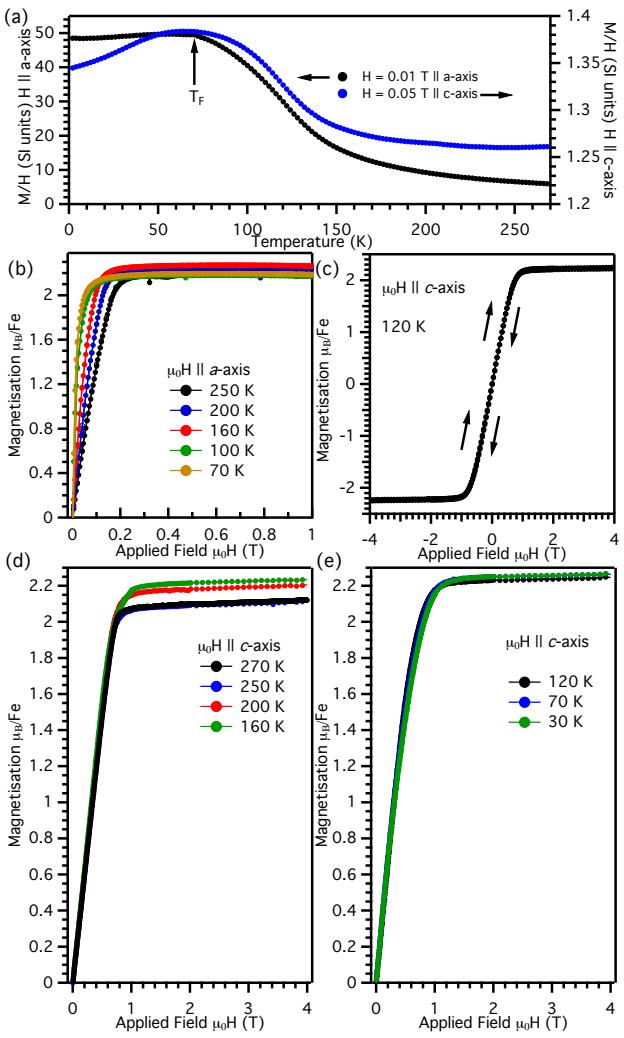

FIG. 2: **(a)** Curves of magnetic D.C. susceptibility (M/H) against temperature, for $\mu_0 H = 0.01$ T and 0.05 T applied || to the a-axis (left axis) and c-axis (right axis) respectively. The maximum in (M/H) attributed to $T_F = 70$ K is indicated. **(b)** The 1 T $\rightarrow$ 0 T segment of hysteresis curves for $\mu_0 H$ || to the a-axis at a series of temperatures. **(c)** The full magnetic hysteresis curve at 120 K between ± 4 T, for $\mu_0 H$ || to the c-axis. No notable hysteresis is observed. **(d)-(e)** The 4 T $\rightarrow$ 0 T segment of hysteresis curves at a series of temperatures for $\mu_0 H$ || to the c-axis.

silica ampoule. The ampoule was evacuated to a pressure of 10^{-6} mbar and sealed. After heating at a rate of 1 °C min^{-1} in a two-zone furnace to temperatures of 650 and 720 °C, the reaction was left for 8 days and yielded crystals up to 6 mm in diameter. Typical single crystals are hexagonal or triangular in shape, with dimensions of ≈ 0.5 mm $\times 0.5$ mm $\times 0.04$ mm, as shown in Figure 1 (c). X-ray Laue diffraction confirmed the c-axis is perpendicular to the plane while the a and b axes are parallel to the edges of the hexagon.

Magnetisation measurements were carried out on a high quality single crystal (RRR = 28, Figure 3 (a))

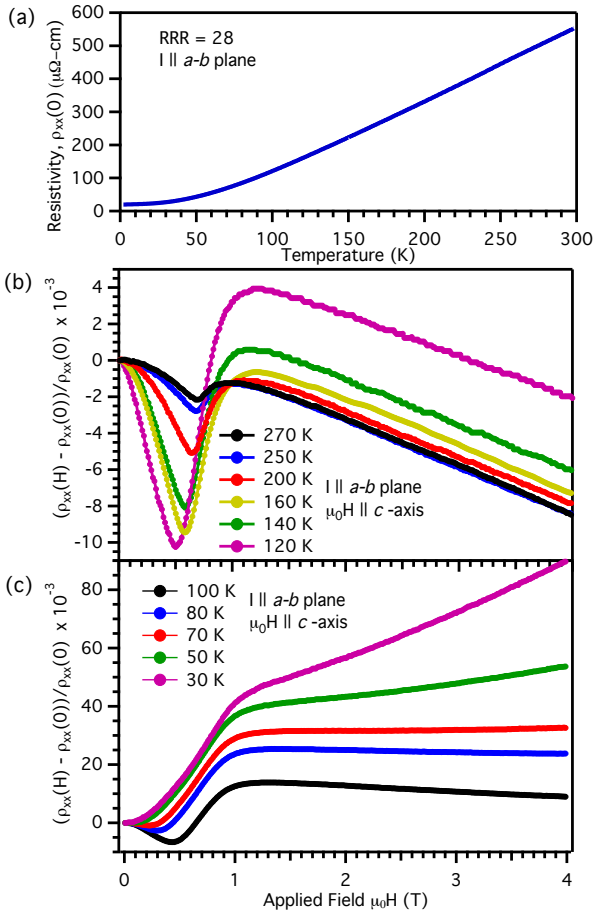

FIG. 3: **(a)** The zero field resistivity, $\rho_{xx}(0)$, of Fe_2Sn_3 measured in the a-b plane of the crystal. **(b)** and **(c)** Curves of the change in resistivity relative to the zero field value against $\mu_0 H$ for a range of temperatures between 270 K and 30 K.

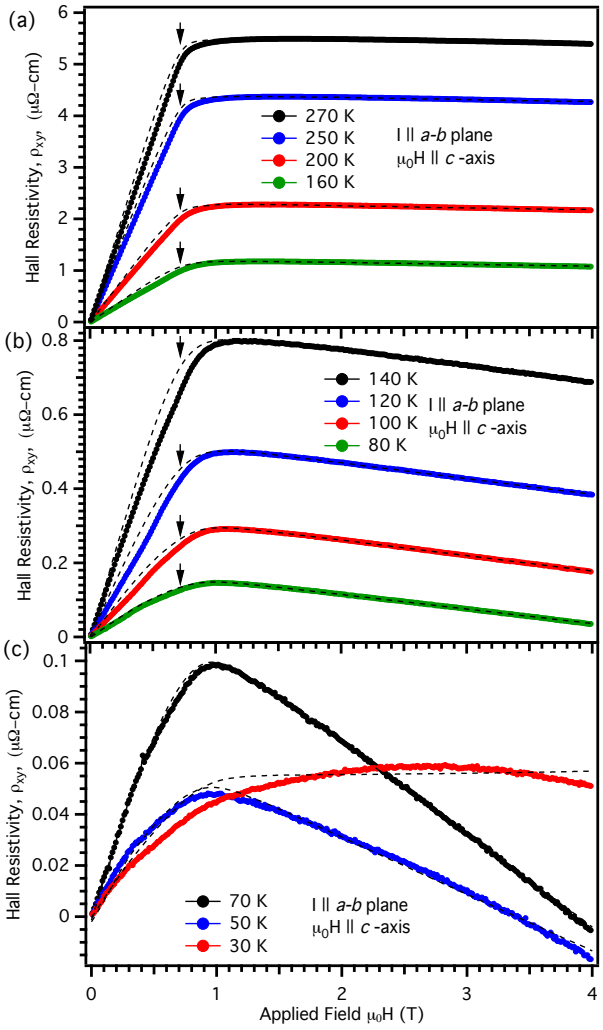

FIG. 4: **(a)-(c)** Curves of Hall resistivity, ρ_{xy}, against $\mu_0 H$, between 270 K and 30 K. Black dashed lines are calculated fits based on EQNS (1) and (2) discussed in the main text. The black arrows indicate the region where an extra contribution to the Hall resistivity, $\Delta\rho_{xy}$, exists.

using a MPMS-XL7, Quantum Design, Inc. SQUID magnetometer. The DC susceptibility, (M/H), namely the magnetisation M divided by $\mu_0 H$, is shown in SI units as a function of temperature from 300 K to 2 K for $\mu_0 H = 0.05$ T || to the c-axis (blue) and $\mu_0 H = 0.01$ T || to the a-axis (black). Hysteresis curves were carried out at constant temperature, following the $\mu_0 H$ ramp profile of 0 T $\rightarrow$ 4 T $\rightarrow$ -4 T $\rightarrow$ 0 T. The 1 T $\rightarrow$ 0 T and 4 T $\rightarrow$ 0 T segments of the hysteresis curves for $\mu_0 H$ || to the a-axis and c-axis respectively, expressed in Bohr magnetons per Fe are shown in Figure 2 (b) and (d)-(e). At all measured temperatures and field directions no notable hysteresis is observed and the curves for increasing and decreasing fields are indistinguishable as shown in the full ± 4 T hysteresis curve in Figure 2 (c) at 120 K for $\mu_0 H$ || to the c-axis.

Gold 25 μm contacts were added along and across the a-b plane of the same sample used in the magnetisation study in a Hall bar geometry, perpendicular to the c-axis, using Dupont 4929 silver epoxy. A current of 200 μA was applied in the a-b plane at a frequency of 37 Hz and the voltage signal measured using a transformer and lock-in amplifier. The zero field resistivity, $\rho_{xx}(0)$, against temperature is shown in Figure 3 (a), demonstrating metallic like behaviour and a sample RRR = 28. The magnetoresistance, $\rho_{xx}(H)$, and Hall resistivity, ρ_{xy}, were measured concurrently in the a-b plane at constant temperature with $\mu_0 H$ || to the c-axis following an identical ± 4 T ramp profile used in the magnetisation study. The $\rho_{xx}(H)$ and ρ_{xy} curves were symmetrised and antisymmetrised respectively, for positive and negative fields to correct for any contact misalignment. The measured curves of the change in resistivity relative to the zero field value i.e. $(\rho_{xx}(H) - \rho_{xx}(0))/\rho_{xx}(0)$, against $\mu_0 H$ up to 4 T are shown in Figure 3 (b) and (c). The corresponding ρ_{xy} curves are shown in Figure 4.

In a collinear ferromagnet ρ_{xy} is made up of (i) the ordinary Hall effect, ρ_{xy}^{n}, dependent on n, the free carrier concentration and (ii) the AHE, ρ_{xy}^{AHE}, dependent on sample magnetisation, M, to give

$$\rho_{xy} = \rho_{xy}^{n} + \rho_{xy}^{AHE} = -\frac{\mu_0 H}{ne} + R_s M, \qquad (1)$$

where e is the elementary charge constant and R_s is the anomalous Hall coefficient. The first microscopic description of the AHE by Karplus and Luttinger [16], known as the intrinsic AHE, depended solely on the topology of the material's band structure including the spin-orbit interaction. In modern notation, the intrinsic effect is expressed in terms of Berry curvature given by

$$R_s = \frac{e^2}{\hbar}\langle\Omega\rangle\rho_{xx}^2 = S_H\rho_{xx}^2. \qquad (2)$$

Here $\langle\Omega\rangle$ is the total weighted average Berry curvature for the band structure and S_H is a temperature independent scaling factor. A non-zero $\langle\Omega\rangle$ causes carriers to experience an extra anomalous Hall velocity perpendicular to applied electric field [17].

There are also 2 extrinsic contributions to R_s, denoted skew and side-jump scattering. Here the spin orbit interaction causes asymmetrical scattering of conduction electron wavepackets from impurities [18, 19]. This asymmetry leads to a Hall voltage that scales linearly with the longitudinal resistivity, $\propto \rho_{xx}$ for skew scattering and quadratically, $\propto \rho_{xx}^2$ for side-jump scattering. Hence there is a difficultly in experimentally distinguishing between intrinsic and side-jump contributions. In transition metal ferromagnets such as *bcc* Fe, that possess non-simplistic band structures and large Berry curvature, the intrinsic AHE is thought to far outweigh the side-jump mechanism [20].

Fits according to EQNS (1) and (2) to determine ρ_{xy}^{n} and ρ_{xy}^{AHE} contributions to ρ_{xy} in Fe_3Sn_2 using the measured curves of M and $\rho_{xx}(H)$ and taking into account demagnetising fields were carried out as follows. The magnetisation curves show moments become aligned with $\mu_0 H \parallel$ to the c-axis above a saturation field $H \geq H_s$ (≈ 1 T). The slope of the hysteresis curves below H_s in Figure 2 (d) and (e) are almost temperature independent and determined by the demagnetisation factor, N. For our sample geometry the expected demagnetising factor is calculated to be $N = 0.796$ [21]. An experimental upper limit for N can be obtained from the maximum slope of dM/dH to give $N < 0.721$ from the data at 270 K. The value of 0.721 was used to estimate the effective field $\mu_0 H_{\text{eff}}$ correcting for the demagnetising field,

$$\mu_0 H_{\text{eff}} = \mu_0 H - NM. \qquad (3)$$

Since the same sample and field history was used in the magnetisation, magnetoresistance and Hall effect measurements, N and hence $\mu_0 H_{\text{eff}}$ has the same value for all these quantities. Below the saturation field, $\mu_0 H_{\text{eff}}$ is close to zero and the Hall resistivity is dominated by terms depending only on the value of M, principally the anomalous Hall term. Above the saturation field, a straightforward fit to ρ_{xy} vs $\mu_0 H_{\text{eff}}$ based on EQNS (1) and (2) is made. This is independent of any dependence of N on the value of M, since M is the same in both measurements. If the scaling factor S_H is considered to be field independent, fits to ρ_{xy} given by EQNS (1) and (2) can then be calculated over the full field range of $\mu_0 H_{\text{eff}}$ and are shown by the dashed lines in Figure 4. The values of n and S_H determined from the fits are shown as a function of temperature in Figure 5 (a). The differences between ρ_{xy} and the calculated value, are discussed in more detail below.

DISCUSSION

We first consider the transition to the spin glass state at T_F. Previous reports saw a transition at $T_F \approx 80$ K, where T_F was determined by a maximum in magnetic susceptibility [6]. Here a similar maximum in the DC magnetic susceptibility, M/H, along both a and c-axis directions is indicated by the arrow in Figure 2 (a). We define T_F as the temperature at which M/H reaches the maximum, giving $T_F = 70 \pm 2.5$ K. Additionally the curves of magnetoresistance in Figure 3 (b)-(c) show a large negative anomaly for $\mu_0 H < 1$ T that becomes suppressed below 70 K and the calculated values of n and S_H from the Hall effect fitting strongly increase below 70 K, Figure 5 (a). The difference in T_F from previous reports may be due to their polycrystalline samples being of a lower quality, extra demagnetising effects from the random grain orientations or the presence of extra strains/dislocations.

Above T_F excellent agreement is seen between ρ_{xy} and the fit to EQNS (1) and (2) for $\mu_0 H > H_s$ (≈ 1 T). However below T_F the fits become progressively worse on cooling, for example the curves at 50 K and 30 K in Figure 4 (c). The poor fitting may be due to an unconventional AHE or a change in Fermi surface in the spin glass state.

The remainder of this letter focuses on temperatures above T_F. At fields below saturation ($\mu_0 H < H_s$) a significant deviation between the fit and data, indicated by the black arrows in Figure 4 (a) and (b) exists. This region in Fe_3Sn_2 is expected to contain non-collinear moments possessing both a-b plane and c-axis components which here we label the R-state. The difference between ρ_{xy} and calculated fits is denoted, $\Delta\rho_{xy}$. Whilst extrinsic responses are expected to become more prominent as the temperature is lowered due to longer relaxation times, including a skew scattering term, $a\rho_{xx}(H)$, where a is a scaling constant, does not reduce $\Delta\rho_{xy}$. Fermi

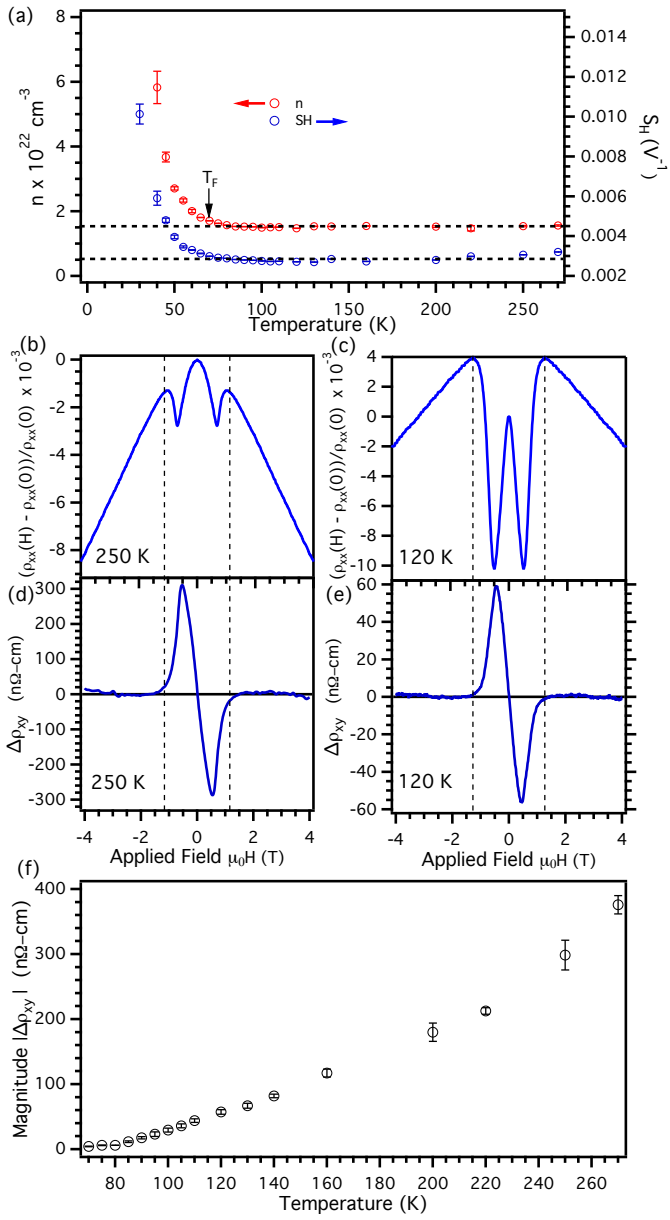

FIG. 5: **(a)** Values of n (left axis) and S_H (right axis) from fits to the Hall resistivity as a function of temperature. The horizontal dashed lines are guides to the eye to demonstrate the temperature independence of n and S_H above T_F. **(b)-(c)** Curves of the change in resistivity relative to the zero field value against $\mu_0 H$ for 250 K and 120 K respectively. **(d)-(e)** The corresponding $\Delta\rho_{xy}$ curves. The vertical dashed lines are guides to the eye showing $\Delta\rho_{xy}$ exists over the same $\mu_0 H$ range as the anomaly seen in magnetoresistance. **(f)** The magnitude of the peak maximum $|\Delta\rho_{xy}|$ averaged for both positive and negative fields as a function of temperature from 270 K to T_F.

surface measurements and band structure calculations for Fe_3Sn_2 show a multi-band system with a complex Fermi surface and large Berry curvature [22–24]. Along with the temperature independence of S_H and n above T_F in Figure 5 (a), it can be concluded that the AHE is intrinsic in accordance with previous reports [10, 25].

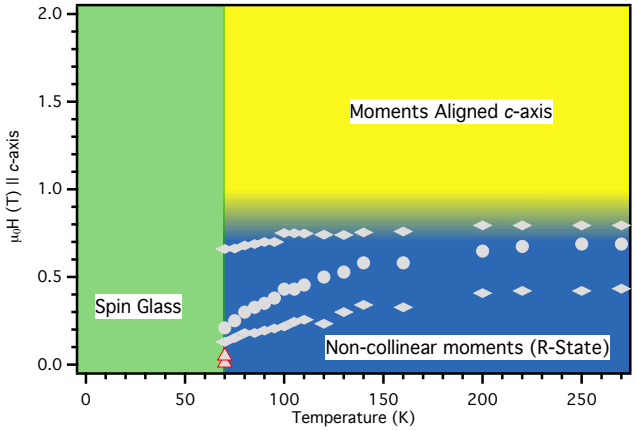

FIG. 6: The $\mu_0 H$-T phase diagram of Fe_3Sn_2 with $\mu_0 H$ || to the c-axis. The green region represents the spin-glass phase below $T_F = 70$ K determined from the magnetic susceptibility, shown as grey triangles outlined in red. Grey circle and diamond markers are derived from the anomaly in magnetoresistance, as described in the main text. Blue depicts the R-state region of non-collinear moments while yellow represents moment saturation with $\mu_0 H$ and shaded blue/yellow represents the cross over region.

Although side-jump scattering also scales with ρ_{xx}^2, for such a multi band system the intrinsic effect is expected to far out weigh any side-jump contribution.

Curves of $\Delta\rho_{xy}$, are shown in units of nΩ-cm against $\mu_0 H$ in Figure 5 (d) and (e) for 250 K and 120 K respectively, while the magnitude of the peak maximum $|\Delta\rho_{xy}|$ averaged for both positive and negative fields is plotted as a function of temperature in Figure 5 (f). The field range over which $\Delta\rho_{xy}$ exists corresponds directly to that of the negative anomaly in magnetoresistance, shown in Figure 5 (b) and (c). Such negative magnetoresistance anomalies in non-collinear magnetic materials may be associated with the presence of magnetic fluctuations, that increase resistivity, being suppressed as moments become aligned with $\mu_0 H$ [26].

The $\Delta\rho_{xy}$ present in the R-state of Fe_3Sn_2 may represent a THE like that in the Skyrmion lattice of MnSi [4]. While the magnitude of $\Delta\rho_{xy}$ (≈ 180 nΩcm at 200 K) is significantly larger and opposite in sign to than that seen for MnSi [4], it is comparable to the THE of MnGe where the period of the chirality is much shorter and a large negative THE exists below 60 K [27]. As discussed in the introduction Lorentz transmission electron microscopy measurements detected spin textured magnetic bubbles topologically equivalent to Skyrmions in Fe_2Sn_3 from 380 K - 130 K up 1.1 T, coinciding well with the temperature and field range the largest $\Delta\rho_{xy}$ effect is seen here. On cooling towards T_F the density of the spin textured magnetic bubbles was observed to decrease [7, 8]. The magnetisation curves in Figure 2 (b) show a decrease in the saturation field approaching T_F indicative of an increase in a-b moment. These observations may provide an explanation for the decreasing

magnitude of $\Delta\rho_{xy}$ on cooling and suggest the need for a significant c-axis component of non-collinear moments for $\Delta\rho_{xy}$ to exist. Similarly since the R-state contains moments with both a-b plane and c-axis components, a decrease in magnitude is expected for temperatures higher than those accessible here that contain a smaller a-b moment component. Then $|\Delta\rho_{xy}|$ will follow a dome shaped dependence to higher temperatures. A THE of a similar magnitude and temperature dependence has recently been reported in $Mn_{1.5}PtSn$ [28].

The magnetic phase diagram of Fe_3Sn_2 for $\mu_0 H$ || c-axis is shown in Figure 6. The transition to the spin-glass phase is shown as the green region where the red outlined grey triangles indicate T_F determined from magnetic susceptibility. The vertical line defining the field dependence of T_F is inferred from the behaviour of the Hall and magnetoresistance signals being clearly different to the left and right of this line as shown in Figure 3 (c) and Figure 4 (c). A vertical line is also reported in the literature by Hou *et al.* [7]. The grey circle and diamond markers represent the minimum and half maxima of the anomaly in magnetoresistance respectively. The blue and yellow regions indicate the R- and fully aligned states respectively whilst the shaded blue/yellow represents the cross over region. The cross over is defined as the region between the second half maxima in the anomaly of magnetoresistance and the saturation field H_s.

Other contributions to $\Delta\rho_{xy}$ not due to a THE should also be considered. The lack of any measurable hysteresis and high value of the RRR suggest the existence of $\Delta\rho_{xy}$ is not due to magnetic domains or disorder. As already discussed $\Delta\rho_{xy}$ is not due to skew scattering and the side-jump mechanism is expected to be far outweighed by the intrinsic effect. The fitting used here assumes a linear ordinary Hall effect response without consideration of different carrier types or multi-band effects. However for fields above moment saturation where the ordinary Hall effect dominates, the linear response fits well with only electron carriers, as shown by the small error bars in n above T_F. In addition to this the temperature independence of n and S_H above T_F suggests any changes in Fermi surface topology here are unlikely.

CONCLUSIONS

In summary we have detected an extra contribution in the Hall resistivity of Fe_3Sn_2 above T_F that may be due to the topological nature of spin textures present in the non-collinear moment R-state below moment saturation. This is the first report of such an anomaly in Fe_3Sn_2 and the first of its kind in a kagome structured material. The feature in Hall resistivity is complimented by a negative anomaly in magnetoresistance.

ACKNOWLEDGEMENTS

Support from the Engineering and Physical Sciences Research Council, EP/P013686 and EP/J00099X (C.D.O'N.) and (A.D.H.), is acknowledged.

[1] P. Bruno, V. K. Dugaev, and M. Taillefumier, Phys. Rev. Lett. **93**, 096806 (2004).
[2] S. Mühlbauer, B. Binz, F. Jonietz, C. Pfleiderer, A. Rosch, A. Neubauer, R. Georgii, and P. Böni, Science **323**, 915 (2009).
[3] Y. Taguchi, Y. Oohara, H. Yoshizawa, N. Nagaosa, and Y. Tokura, Science **291**, 2573 (2001).
[4] A. Neubauer, C. Pfleiderer, B. Binz, A. Rosch, R. Ritz, P. G. Niklowitz, and P. Böni, Physical Review Letters **102**, 186602 (2009).
[5] R. Ritz, M. Halder, C. Franz, A. Bauer, M. Wagner, R. Bamler, A. Rosch, and C. Pfleiderer, Physical Review B **87**, 134424 (2013).
[6] L. A. Fenner, A. A. Dee, and A. S. Wills, Journal of Physics: Condensed Matter **21**, 452202 (2009).
[7] Hou, Z. Ren, W. Ding, B. Xu, G. Wang, Y. Yang, B. Zhang, Qi. Zhang, Y. Liu, E. Xu, F. Wang, W. Wu, G. Zhang, X. Shen, B. and Zhang, Z., Advanced Materials, **29**, 1701144 (2017).
[8] J.-X. Yin, S. S. Zhang, H. Li, K. Jiang, G. Chang, B. Zhang, B. Lian, C. Xiang, I. Belopolski, H. Zheng, et al., Nature **562**, 91 (2018).
[9] B. Malaman and B. Roques, Acta Cryst. **B32**, 1348 (1976).
[10] Q. Wang, S. Sun, X. Zhang, F. Pang, and H. Lei, Phys. Rev. B **94**, 075135 (2016).
[11] G. Trumpy, E. Both, C. Djéga-Mariadassou, and P. Lecocq, Phys. Rev. B **2**, 3477 (1970).
[12] G. L. Caer, B. Malaman, and B. Roques, Journal of Physics F: Metal Physics **8**, 323 (1978).
[13] G. L. Caer, B. Malaman, L.Haggstrom, and T. Ericsson, Journal of Physics F: Metal Physics **9**, 1905 (1979).
[14] B. Malaman, D. Fruchart, and G. L. Caer, Journal of Physics F: Metal Physics **8**, 2389 (1978).
[15] M. Pereiro, D. Yudin, J. Chico, C. Etz, O. Eriksson, and A. Bergman, Nat Commun **5** (2014).
[16] R. Karplus and J. M. Luttinger, Phys. Rev. **95**, 1154 (1954).
[17] M. Lee, Y. Onose, Y. Tokura, and N. P. Ong, Physical Review B **75**, 172403 (2007).
[18] J. Smit, Physica **24**, 39 (1958).
[19] L. Berger, Phys. Rev. B **2**, 4559 (1970).
[20] Y. Yao, L. Kleinman, A. H. MacDonald, J. Sinova, T. Jungwirth, D.-S. Wang, E. Wang, and Q. Niu, Phys. Rev. Lett. **92**, 037204 (2004).
[21] R. B. Goldfarb and J. V. Minervini, Review of Scientific Instruments **55**, 761 (1984).
[22] L. Ye, M. Kang, J. Liu, F. von Cube, C. R. Wicker, T. Suzuki, C. Jozwiak, A. Bostwick, E. Rotenberg, D. C. Bell, et al., Nature **555**, 638 EP (2018).
[23] L. Ye, M. K. Chan, R. D. McDonald, D. Graf, M. Kang, J. Liu, T. Suzuki, R. Comin, L. Fu, and J. G. Checkelsky, arXiv **1809.11159** (2018).
[24] Z. Lin, J.-H. Choi, Q. Zhang, W. Qin, S. Yi, P. Wang, L. Li, Y. Wang, H. Zhang, Z. Sun, et al., Phys. Rev. Lett. **121**, 096401 (2018).
[25] T. Kida, L. A. Fenner, A. A. Dee, I. Terasaki, M. Hagiwara, and A. S. Wills, Journal of Physics: Condensed Matter **23**, 112205 (2011).

[26] G. Abdul-Jabbar, D. A. Sokolov, C. D. O'Neill, C. Stock, D. Wermeille, F. Demmel, F. Krüger, A. G. Green, F. Lévy-Bertrand, B. Grenier, et al., Nature Physics **11**, 321 EP (2015).
[27] N. Kanazawa, Y. Onose, T. Arima, D. Okuyama, K. Ohoyama, S. Wakimoto, K. Kakurai, S. Ishiwata, and Y. Tokura, Phys. Rev. Lett. **106**, 156603 (2011).
[28] P. Swekis, A. Markou, D. Kriegner, J. Gayles, R. Schlitz, W. Schnelle, S. T. B. Goennenwein, and C. Felser, Phys. Rev. Materials **3**, 013001 (2019).